HHS Public Access

Author manuscript

J Neuropathol Exp Neurol. Author manuscript; available in PMC 2017 January 04.

Published in final edited form as:

J Neuropathol Exp Neurol. 2013 September ; 72(9): 833–845. doi:10.1097/NEN.0b013e3182a23506.

Skeletal Muscle Biopsy Analysis in Reducing Body Myopathy and Other *FHL1*-Related Disorders

Edoardo Malfatti, MD, **Montse Olivé, MD**, **Ana Lía Taratuto, MD, PhD**, **Pascale Richard, PhD**, **Guy Brochier, PhD**, **Marc Bitoun, PhD**, **Lucie Gueneau, PhD**, **Pascal Laforêt, MD, PhD**, **Tanya Stojkovic, MD**, **Thierry Maisonobe, MD**, **Soledad Monges, MD**, **Fabiana Lubieniecki, MD**, **Gabriel Vasquez, MD**, **Nathalie Streichenberger, MD**, **Emmanuelle Lacène, MSc**, **Maria Saccoliti, MD**, **Bernard Prudhon, MSc**, **Marilena Alexianu, MD**, **Dominique Figarella-Branger, MD**, **Joachim Schessl, MD**, **Carsten Bonnemann, MD**, **Bruno Eymard, MD, PhD**, **Michel Fardeau, MD**, **Gisèle Bonne, PhD**, and **Norma Beatriz Romero, MD, PhD**

Unité de Morphologie Neuromusculaire, Institut de Myologie, Groupe Hospitalier Universitaire La Pitié-Salpêtrière, Paris, France (EM, MO, GB, EL, MF, NBR); Department of Neurological, Neurosurgical, and Behavioral Sciences, University of Siena, Siena, Italy (EM); INSERM, Paris, France (EM, MB, LG, BP, GB, NBR); Université Pierre et Marie Curie, Institut de Myologie, Paris, France (EM, MB, LG, BP, GB, NBR); Centre de référence de Pathologie Neuromusculaire Paris-Est, Institut de Myologie, Paris, France (EM, PL, TS, BE, NBR); Institut de Neuropatologia, IDIBELL-Hospital de Bellvitge, Barcelona, Spain (MO); Hospital Nacional de Pediatría J.P. Garrahan, and Instituto de Investigaciones Neurologicas, FLENI, Buenos Aires, Argentina (ALT, SM, FL, GV, MS); AP-HP, GHU La Pitié-Salpêtrière, U.F. Cardiogénétique et Myogénétique, Service de Biochimie Métabolique, Paris, France (PR, GB); Département de Neurophysiologie Clinique, Assistance Publique-Hôpitaux de Paris, Paris, France (TM); Hospices Civils de Lyon, Centre de Pathologie Est, Université Claude Bernard Lyon, Lyon, France (NS); Bucharest, Romania (MA); AP-HM, CHU Timone, Neuro-oncology Team, Aix-Marseille University, Marseille, France (DFB); INSERM, Aix-Marseille University, Marseille, France (DFB); Friedrich-Baur-Institute, Department of Neurology, Ludwig-Maximilians University of Munich, Munich, Germany (JS); and Neurogenetics Branch, National Institute of Neurological Disorders and Stroke, National Institutes of Health, Bethesda, Maryland (CB).

Abstract

FHL1 mutations have been associated with various disorders that include reducing body myopathy (RBM), Emery-Dreifuss–like muscular dystrophy, isolated hypertrophic cardiomyopathy, and some overlapping conditions. We report a detailed histochemical, immunohistochemical, electron microscopic, and immunoelectron microscopic analyses of muscle biopsies from 18 patients carrying mutations in *FHL1*: 14 RBM patients (Group 1), 3 Emery-Dreifuss muscular dystrophy patients (Group 2), and 1 patient with hypertrophic cardiomyopathy and muscular hypertrophy (Group 2). Group 1 muscle biopsies consistently showed RBs associated with cytoplasmic bodies. The RBs showed prominent FHL1 immunoreactivity whereas desmin, αB-crystallin, and myotilin immunoreactivity surrounded RBs. By electron microscopy, RBs were composed of electron-

Send correspondence and reprint requests to: Norma Beatriz Romero, MD, PhD, Institut de Myologie, INSERM UMR 974, GHU La Pitié-Salpêtrière, Paris, France; nb.romero@institut-myologie.org.

dense tubulofilamentous material that seemed to spread progressively between the myofibrils and around myonuclei. By immunoelectron microscopy, FHL1 protein was found exclusively inside RBs. Group 2 biopsies showed mild dystrophic abnormalities without RBs; only minor nonspecific myofibrillar abnormalities were observed under electron microscopy. Molecular analysis revealed missense mutations in the second FHL1 LIM domain in Group 1 patients and ins/del or missense mutations within the fourth FHL1 LIM domain in Group 2 patients. Our findings expand the morphologic features of RBM, clearly demonstrate the localization of FHL1 in RBs, and further illustrate major morphologic differences among different *FHL1*-related myopathies.

Keywords

Congenital myopathies with protein aggregates; *FHL1*; *FHL1*-related myopathies; Protein surplus myopathies; Reducing bodies

INTRODUCTION

The FHL1 protein isoforms FHL1A, FHL1B, and FHL1C are encoded by alternative splicing of the *FHL1* gene on Xq26 chromosome (1). They contain LIM domains, highly conserved sequences constituted by cysteine-rich double zinc-finger motifs that mediate protein binding (2). FHL1A (generally named FHL1) is a 32-kd protein composed of 4.5 LIM domains that is highly expressed in skeletal and cardiac muscle (3). In skeletal muscle, FHL1 localizes to the I-band and M-line of the sarcomere, the sarcolemma, and the nucleus (4). FHL1B (SLIMMER/KyoT3, 36 kd) and FHL1C (KyoT2, 22 kd) contain different C-terminal domains and (because of alternative splicing) 3.5 and 2.5 LIM domains, respectively. They are expressed in skeletal and cardiac muscle to a lesser extent compared with FHL1A (1, 5–7).

Mutations in *FHL1* (OMIM 300163) have been as sociated with different disorders, including reducing body myopathy (RBM), X-linked–dominant scapuloperoneal myopathy, X-linked myopathy with postural muscle atrophy (XMPMA), rigid spine syndrome, Emery-Dreifuss muscular dystrophy (EDMD), isolated hypertrophic cardiomyopathy (HCM), and some overlapping conditions (1, 8). *FHL1*-related disorders may be divided into 2 main subgroups based on the muscle pathology. The first is characterized by the presence of RBs in muscle fibers and includes RBM, X-linked–dominant scapuloperoneal myopathy, and rigid spine syndrome. The presence of RBs as a constant morphologic feature suggests that these conditions may be considered as a spectrum of 1 unique entity that is best subsumed under “RBM.” The second group does not exhibit RBs in muscle biopsies and includes patients with EDMD, XMPMA, and the recently described *FHL1*-related isolated HCM (1, 8). Exceptions to this classification seem to exist after the recent identification of RBs in muscle biopsies of 2 brothers with late-onset XMPMA (9).

Reducing bodies were first described more than 35 years ago as cytoplasmic inclusions that reduce nitro-blue tetrazolium (NBT), thus staining strongly in menadione-NBT reaction (10). Pioneer studies speculated that the reducing activity is likely caused by the presence of sulphydryl groups (11). Moreover, the close relationship between the myofilaments and the

RB granular material may indicate the possibility that the granules arise from some myofibrillar component (11). Recent proteomic studies have demonstrated that RBs correspond to protein aggregates, one of the major constituents of which is FHL1 (12); however, the presence of FHL1 inside RBs has never been demonstrated in human muscle tissue by immunoelectron microscopy (IEM).

Reducing body myopathy patients generally harbor missense mutations affecting conserved residues of FHL1 essential for the proper protein folding and stabilization of the LIM2 domain (1). Patients without RBs harbor mutations located in the most distal exons affecting differently the 3 FHL1 isoforms (13–15).

To enhance understanding of the mechanisms that produce the morphologic phenotype of different FHL1-related myopathies, we studied 18 patients carrying a mutation in *FHL1*, including 14 RBM, 3 EDMD, and 1 patient with HCM and muscular hypertrophy patients using immunohistochemistry, EM, and IEM. Our results expand the pathologic spectrum of RBM, directly demonstrate localization of FHL1 in RBs, and further illustrate major morphologic differences between different clinical forms of *FHL1*-related myopathies.

MATERIALS AND METHODS

Patients

Eighteen patients (i.e. 14 RBM patients, 3 EDMD, and 1 patient with HCM and muscle hypertrophy) from 16 unrelated families were included in the present study. Patients P1, P2, P3, P5, P6, P7, P8, P9, P14, and P15 (n = 10) are reported herein for the first time. They belong to 6 unrelated families from France, Romania, and Argentina. Patients P5 and P7 are sons of P6 and P8, respectively. Clinical and pathologic data from patient P4 were reported before the causative gene for RBM was discovered (16). Data on the clinical phenotype, pathologic features, and genetic characterization of 7 patients, 4 with RBM (P10, P11, P12, P13), and 3 with an EDMD phenotype (P16, P17, and P18) have been previously described (13, 17).

Mutation Analysis

Patients or parents gave informed consent for the genetic analysis according to French legislation. Genomic DNA was extracted from blood samples by standard methods. DNAs were studied by direct sequencing of exons and intronexon boundaries of *FHL1* gene, as previously described (13).

Morphologic Studies

An open muscle biopsy was performed in all patients after informed consent. Age at biopsy varied from 10 months to 58 years (Table). For conventional histochemical techniques, 10-μm-thick cryostat sections were stained with hematoxylin and eosin (H&E), modified Gomori trichrome, periodic acid-Schiff technique, Oil red O, reduced nicotinamide adenine dinucleotide dehydrogenase–tetrazolium reductase, succinic dehydrogenase (SDH), cytochrome oxidase (COX), and adenosine triphosphatase (ATPase) preincubated at pH 9.4, 4.63, and 4.35. The presence of RBs was assessed in muscle sections processed for the

menadione–nitro blue tetrazolium with or without α-glycerophosphate. Digital photographs of each biopsy were obtained with a Zeiss AxioCam HRc linked to a Zeiss Axioplan Bright Field Microscope and processed with the Axio Vision 4.4 software (Zeiss, Germany).

Immunohistochemistry and Double Immunofluorescence

Frozen muscle samples for immunohistochemical and immunofluorescence analyses were available only for 1 patient with RBM (P1) and for 3 patients from Group 2 (P16, P17, and P18). Frozen muscle was not available for the other patients.

Immunohistochemistry with antibodies to desmin (D33, 1:1000, Dako-Desmin; DakoCytomation, Glostrup, Denmark), αB-crystallin (NCL-ABCrys-512, 1:300; Novocastra, Newcastle, UK), and myotilin (NCL-Myotilin, 1:50; Novocastra) was performed on 8-μm-thick cryosections using an immunoperoxidase-automated procedure (Ventana, Illkirch, France). Subsequently, sections were incubated with an appropriate conjugated secondary antibody for 1 hour, and the sections were slightly counterstained with H&E.

For double labeling immunofluorescence staining, 6-μm-thick sections were fixed in cold acetone for 10 minutes. They were then incubated with anti-FHL1 antibody (ab49241, 1:100; Abcam, Cambridge, UK) overnight at 4°C as the first antibody and subsequently with anti-desmin (D33, 1:1000) as the second antibody. Subsequently, sections were incubated with appropriate conjugated secondary antibodies for 1 hour. A set of control slides was prepared, with omission of the primary antibodies.

Electron Microscopy

Detailed electron microscopy analysis was performed on samples from the entire cohort. Small muscle specimens were fixed in glutaraldehyde (2.5%, pH 7.4), postfixed with 2% OsO_4, dehydrated, and embedded in resin (EMBed-812; Electron Microscopy Sciences, Hatfield, PA). Ultrathin sections from at least 3 small blocks from each patient were stained with uranyl acetate and lead citrate. The grids were observed using a Philips CM120 electron microscope (80 kV; Philips Electronics NV, Eindhoven, The Netherlands) and were photodocumented using a Morada camera (Soft Imaging System, France).

Immunoelectron Microscopy

Immunoelectron microscopy was performed in specimens from 14 patients (P1, P3, P4, P5, P6, P7, P8, P9, P10, P11, P12, P13, P15, and P17) and in an unrelated female subject presenting myalgia without muscle weakness whose biopsy did not have morphologic alterations either by light microscopy or EM (internal control). Muscle biopsies were fixed in a solution of 2% paraformaldehyde, 2.5% glutaraldehyde in 0.12 mol/L phosphate buffer. Small pieces were postfixed for 2 hours in 2% OsO_4 in 0.12 mol/L cacodylate buffer, dehydrated in graded ethanol series and flat embedded in Epon. Ultrathin sections (80 nm) were etched with a saturated aqueous solution of sodium metaperiodate (15 minutes) before performing the immunogold labeling technique. Sections were incubated for 30 minutes in Tris-buffered saline containing 1% bovine serum albumin and 1% normal goat serum and then overnight in the same buffer containing the primary rabbit polyclonal antibody to FHL1

(1:50 dilution). After extensive washes in Tris-buffered saline, the sections were incubated for 3 hours with a gold-conjugated goat anti-rabbit IgG antibody (1:50 dilution; British BioCell, Cardiff, UK). The sections were washed in distilled water, stained with 2% uranyl acetate and lead citrate, and observed with a Philips CM120 transmission electron microscope.

RESULTS

Clinical Features

Ten patients were female and 8 were male. According to the clinical and morphologic phenotype, patients were divided into 2 groups: Group 1 consisted of patients with RBM (P1 to P14), and group 2 consisted of patients with no RBs and presented with HCM with muscle hypertrophy (P15) or an EDMD phenotype (P16 to P18). The age of onset varied from 4 months to 29 years in Group 1 and from 3 weeks to 48 years in Group 2. Clinical summary, laboratory features, a complete list of morphologic methods applied to muscle biopsies, and genetic characterization of all patients is provided in the Table.

Molecular Data

Group 1—The screening of *FHL1* gene in DNA of patients newly analyzed for *FHL1* mutations resulted in identification of 6 previously described *FHL1* mutations (Table; Fig. 1). Patients P1 and P14 had 2 de novo mutations. X-linked transmission was verified in all relevant pedigrees. All the mutations identified in Group 1 are located in exon 5 and change 1 of the 8 zinc-coordinating cysteine or histidine residues of the LIM2 domain (Fig. 1).

Group 2—We identified a novel mutation consisting of a nucleotide deletion c.632delA in exon 6 in P15 (Table). This change introduces a frame shift and a premature stop codon for both FHL1A and FHL1B, eventually leading to C-terminal truncated proteins lacking the LIM4 domain for FHL1A (p.Asp211ValfsX47) (Fig. 1), and the NSL, NES, and RBP-J domains for FHL1B (p.Asp211ValfsX27) (Fig. 1). The *FHL1* mutations found in patients P16, P17, and P18 have been previously described and are located in exon 8, affecting only the LIM4 domain of FHL1A (Fig. 1) (12).

Histologic and Histochemical Features

Group 1—Patients P1 and P5 underwent a first biopsy in a nonaffected muscle that failed to show relevant alterations. The biopsy of P2 was interpreted as nonspecific. All of the other RBM patients showed similar morphologic abnormalities characterized by marked variability in fiber size, hypertrophic and atrophic-rounded fibers, and variable degrees of endomysial fibro–fatty tissue substitution. There were increased numbers of internal nuclei. The abnormalities were always focally distributed: some fascicles appeared severely damaged, whereas others showed only minor abnormalities.

All of the biopsies showed some enlarged nuclei; some of them showed a pale central zone on H&E. In all cases, scattered necrotic fibers, often undergoing phagocytosis, were observed. There was no perivascular or endomysial inflammation. Rimmed vacuoles were present only in the biopsy of patient P6 (not shown). The most striking finding was the

presence of RBs. These appear as bright pink cytoplasmic inclusions on H&E (Fig. 2A). Reducing bodies strongly reduced NBT on menadione staining with or without α-glycerophosphate (Fig. 2B). They were devoid of oxidative activities especially with COX (not shown) and SDH (Fig. 2C) stains. The number and sizes of RBs varied among the samples; some fibers were completely replaced by them. The numbers of RBs and the severity of pathologic abnormalities observed in each biopsied muscle did not seem to correlate with the degree of disease severity or with duration of disease manifestations. In addition, several muscle fibers contained a mixture of amorphous and granular material that did not react with the menadione-NBT staining. Furthermore, cytoplasmic bodies were seen as collections of red granules on modified Gomori trichrome in the cytoplasm of several fibers. Adenosine triphosphatase staining revealed type 1 fiber predominance in all cases. In a single patient, there were single or multiple well-demarcated zones devoid of oxidative enzyme activity that closely resembled cores.

Group 2—Light microscopy findings in patient P15 showed nonspecific abnormalities characterized by mild variability in fiber size, some proliferation of endomysial connective tissue, and a few internal nuclei. No cytoplasmic inclusions or areas of myofibrillar disorganization were identified (not shown). The biopsies of patients P16, P17, and P18 showed only mild dystrophic features (13).

Immunohistochemistry and Immunofluorescence

Group 1 and Group 2—Desmin, myotilin, and αB-crystallin immunoreactivities were absent from the areas corresponding to RBs, but they were enhanced at their periphery, as seen on serial sections processed for menadione-NBT and for these immunostains (Fig. 2B, D–F). Moreover, diffuse desmin, myotilin, and αB-crystallin overexpression was observed in atrophic fibers (Fig. 2D–F).

Immunofluorescence analysis of control muscle sections revealed diffuse FHL1 cytoplasmic expression (Fig. 3A). In contrast, a section from P1 showed that the intracytoplasmic inclusions corresponding to RBs were strongly immunolabeled for FHL1 (Fig. 3B). Interestingly, regions of the fibers in proximity to RBs and adjacent normal fibers showed absence of FHL1 immunoreactivity (Fig. 3B). Muscle biopsy sections from group 2 patients revealed less intense FHL1 immunofluorescence versus controls (Fig. 3C).

Double immunofluorescence analysis with anti-FHL1 and anti-desmin antibodies revealed partial colocalization of both proteins at the periphery of RBs (Fig. 3D, E), diffuse colocalization in atrophic fibers, and no colocalization within RBs (Fig. 3D). Moreover, increased FHL1 immunofluorescence was observed in perinuclear areas (Fig. 3D, F).

Electron Microscopy

Group 1—Biopsies with RBs by light microscopy showed a wide spectrum of ultrastructural features depending on the stage of the lesions; regional distribution of pathologic alterations was also confirmed. Early changes were characterized by the presence of highly osmiophilic granular material seeming to emanate from structures corresponding to the I-band and extending perpendicularly and longitudinally to the sarcomere (Fig. 4A).

Fine filamentous semidense material was also observed near the Z-line and extended along the sarcomere (Fig. 4B). Clusters of mitochondria and glycogen granules were very often observed adjacent to both types of material. In fibers showing more advanced lesions, the osmiophilic coarse tubulofilamentous granular material appeared to spread to the subsarcolemma and between the myofibrils, giving rise to the formation of large inclusions that correspond to the RBs visualized with menadione-NBT staining. Reducing bodies were composed of coarse tubulofilaments (Fig. 4C). Typical cytoplasmic bodies with a dense core and a clear halo of fine filaments were found surrounding or intermingled with the RBs (Fig. 5A, B). In all cases, there was osmiophilic granular/tubulofilamentous material around myonuclei (Fig. 5C–F). Thus, myonuclei invariably appeared to be encased by RBs. In addition, some nuclei showed a number of abnormalities, including apoptotic changes, hypercondensed chromatin, prominent nucleoli, and even the presence of intranuclear osmiophilic granular material.

Most severely damaged fibers showed completely disrupted sarcomeric structures replaced by RBs, cytoplasmic bodies, filamentous material, mini–nemaline rods, autophagic vacuoles, remnants of filaments, lipid droplets, and clusters of enlarged mitochondria.

Several additional abnormalities were observed. The biopsy of patient P13 showed large numbers of fingerprint bodies in several fibers (Fig. 6A, B). Dilated sarcotubular cisternae were observed in 5 patients (P1, P7, P8, P9, and P10), and honeycomb structures were observed in the biopsy of P1 (Fig. 6C). The muscle of patient P13 showed the presence of intranuclear rods (Fig. 6D).

Group 2—Ultrastructural studies demonstrated only minor abnormalities, characterized by nonspecific irregularities of the Z-line. Neither osmiophilic granular deposits nor semidense filamentous material was observed in any case (not shown).

Immunoelectron Microscopy

Our protocol for immune electron microscopy in Epon-embedded muscle sections allowed us to develop a specific gold-labeled FHL1 staining. The IEM analysis conducted in our internal control and in Group 2 patients (P15 and P17) revealed the presence of gold-labeled FHL1 adjacent to the Z-line, I-band, and M-line, corresponding to the expected normal location for FHL1 in unaffected skeletal muscle (Figure, Supplemental Digital Content 1, http://links.lww.com/NEN/A481).

In the biopsies of all 12 Group 1 patients, we found that gold-labeled FHL1 antibody was strongly enriched in the electron-dense inclusion corresponding to RBs (Fig. 7A, B). Reducing body material surrounding nuclei was also enriched with FHL1 immunoreactivity (Fig. 8), and this immunoreactivity clearly corresponded to the perinuclear labeling seen by immunofluorescence (Fig. 3D, F). Moreover, the cytoplasmic bodies intermingled with RB material never stained with FHL1 antibody (Fig. 9). In the more preserved areas of the

Supplemental digital content is available for this article. Direct URL citation appear in the printed text and is provided in the HTML and PDF versions of this article on the journal's Web site (www.jneuropath.com).

muscle biopsies, we also noticed some binding adjacent to the Z-line/I-band/M-line (not shown).

DISCUSSION

We have reported a detailed comparative histologic, immunohistochemical, ultrastructural, and IEM analysis in a large cohort of 18 patients carrying mutations in the *FHL1* gene.

Patients P1 to P14 had severe RBM, and all harbored previously reported mutations located in the LIM2 *FHL1* domain. A striking asymmetric pattern of muscle weakness and atrophy was present in 5 of the female RBM patients whose clinical onset was in late childhood or in early adulthood. Patients P5, P6, P7, and P8 are sons and mothers affected by the same *FHL1* LIM2 domain mutation. Of interest, the 2 mothers (P6 and P8) manifested a striking asymmetric phenotype compared with their sons. X-linked inactivation studies were not performed in our patients, but variable expression of mutated X allele could result in the different clinical expression encountered in these 2 pedigrees. Thus, *FHL1* mutation screening should be considered in the diagnostic workup of female patients presenting with progressive asymmetric muscle weakness and atrophy with onset in early adult life.

In Group 2 patients, P15 has a novel FHL1A p.Asp211ValfsX47/FHL1B p.Asp211ValsfX27-mutation in exon 6 associated with HCM and muscular hypertrophy. Patients P16, P17, and P18 have an EDMD phenotype associated with mutations modifying differently the 3 FHL1 isoforms, that is, with LIM4 and/or C-terminal and LIM4 domain alterations (13).

Our morphologic analysis allows us to confirm distinct morphologic phenotypes in the 2 groups. Muscle biopsies from patients belonging to Group 2 showed mild dystrophic features but no RBs. By contrast, muscle biopsies from Group 1 patients displayed a consistent pathologic picture, with characteristic histologic findings of round or oval RBs, commonly localized at the outer edge of muscle fibers or surrounding enlarged myonuclei, and cytoplasmic bodies. These 2 different types of inclusions are typically found only in some sectors of the muscle sections (12, 17, 18). For this reason, the choice of a clinically affected muscle as the site for a biopsy is critical for maximizing the probability of encountering RBs and cytoplasmic bodies, the pathologic changes associated with RBM. This is the first observation of fingerprint bodies and intranuclear rods associated with RBM. Immunofluorescence studies in P1 confirmed the presence of increased FHL1 immunoreactivity in RB areas and in atrophic fibers. A complete absence of FHL1 immunostaining in nonaffected areas of the muscle biopsy was also observed. More interestingly, perinuclear regions of fibers containing RBs showed increased FHL1 reactivity. This is consistent with the accumulation of mutant FHL1B and/or FHL1C nuclear isoforms. In contrast, group 2 patient biopsies showed a homogeneous but less intense sarcomeric distribution compared with that in control muscle.

It has been recently proposed that RBM can show typical features of myofibrillar myopathy (18). Therefore, we performed immunostaining directed against myofibrillary components. Desmin, αB-crystallin, and myotilin-immunoreactive material was present exclusively at the

periphery and constantly absent from RB. Using double immunofluorescence with FHL1 and desmin antibodies, we demonstrated that desmin seems to form scaffold-like structures around RB, a feature characteristic of aggresomes, which are usually “caged” by an intermediate filament network (19). Taken together, our immunohistochemical and ultrastructural analysis indicates that the type and composition of protein aggregates in RBM are markedly different from those found in other myofibrillar myopathy subtypes.

Ultrastructural analysis demonstrated that the initial lesion consisted of tubulofilaments that emerged in the vicinity of the I-band, suggesting that the initial pathologic aggregation process possibly started at the site of normal FHL1 localization. In fibers with more severe morphologic changes, RB material invaded the entire myofiber spreading around the nuclei and dislocating all its components.

Our study does, however, have some limitations because there was not sufficient frozen material to extend our immunofluorescence studies to the entire cohort, and the observations of perinuclear FHL1 staining and ultrastructural evidence of RB material around myonuclei were only correlative. Nevertheless, we wanted to address specific questions regarding FHL1 contributions in RB formation and distribution by IEM. Schessl et al (17) previously described IEM on reembedded frozen material from an RBM patient. The electron-dense inclusion showed some gold-labeled FHL1 enrichment, but the muscular ultrastructure was not well preserved because of the freezing (17). With a different approach using Epon-embedded muscle, we obtained a well-preserved sarcomeric structure, enabling us to address this issue. Indeed, FHL1 was found inside the intermyofibrillar and perinuclear RB. Our data strongly support the idea that LIM2-mutated FHL1 protein deposition could start and possibly precipitate protein aggregation. Further IEM studies aimed at identifying the contribution of different FHL1 isoforms in RB formation are planned.

In addition, we confirmed the expected FHL1 localization in skeletal muscle adjacent to the Z-line, I-band, and M-line (4).

Finally, in this study of a large cohort of *FHL1*-mutated patients, we were able to improve characterization of the pathologic spectrum associated with 2 groups of *FHL1*-related myopathies and demonstrated ex vivo the FHL1 contribution to RB formation. More studies are needed to dissect the pathophysiology of *FHL1*-related myopathies for the development of suitable therapeutic strategies.

Acknowledgments

The authors are very grateful to our team of “Risler Lab.” Their technical performance and secretarial assistance were essential to the success of this work (A. Madelaine, M. Beuvin, D. Chauveau, L. Manéré, MT. Viou, F. Levy-Borsato). The authors thank Dr. M. Nogues and Pr. A. Dubrovsky for referring patient 6 and Dr. Gillian Butler-Browne for proofreading the manuscript.

This work was supported by the Institut National de la Santé et de la Recherche Médicale, the Association Française contre les Myopathies, the Association Institut de Myologie, and the Agence Nationale de la Recherche.

REFERENCES

1. Cowling BS, Cottle DL, Wilding BR, et al. Four and a half LIM protein 1 gene mutations cause four distinct human myopathies: A comprehensive review of the clinical, histological and pathological features. Neuromuscul Disord. 2011; 21:237–251. [PubMed: 21310615]
2. Kadrmas JL, Beckerle MC. The LIM domain: From the cytoskeleton to the nucleus. Nat Rev Mol Cell Biol. 2004; 5:920–931. [PubMed: 15520811]
3. Liang L, Zhang HW, Liang J, et al. KyoT3, an isoform of murine FHL1, associates with the transcription factor RBP-J and represses the RBP-J-mediated transactivation. Biochim Biophys Acta. 2008; 1779:805–810. [PubMed: 18760388]
4. McGrath MJ, Cottle DL, Nguyen MA, et al. Four and a half LIM protein 1 binds myosin-binding protein C and regulates myosin filament formation and sarcomere assembly. J Biol Chem. 2006; 281:7666–7683. [PubMed: 16407297]
5. Brown S, McGrath MJ, Ooms LM, et al. Characterization of two isoforms of the skeletal muscle LIM protein 1, SLIM1. Localization of SLIM1 at focal adhesions and the isoform slimmer in the nucleus of myoblasts and cytoplasm of myotubes suggests distinct roles in the cytoskeleton and in nuclear-cytoplasmic communication. J Biol Chem. 1999; 274:27083–27091. [PubMed: 10480922]
6. Lee SM, Li HY, Ng EK, et al. Characterization of a brain-specific nuclear LIM domain protein (FHL1B) which is an alternatively spliced variant of FHL1. Gene. 1999; 237:253–263. [PubMed: 10524257]
7. Ng EK, Lee SM, Li HY, et al. Characterization of tissue-specific LIM domain protein (FHL1C) which is an alternatively spliced isoform of a human LIM-only protein (FHL1). J Cell Biochem. 2001; 82:1–10. [PubMed: 11400158]
8. Friedrich FW, Wilding BR, Reischmann S, et al. Evidence for FHL1 as a novel disease gene for isolated hypertrophic cardiomyopathy. Hum Mol Genet. 2012; 21:3237–3254. [PubMed: 22523091]
9. Feldkirchner S, Walter MC, Müller S, et al. Proteomic characterization of aggregate components in an intrafamilial variable FHL1-associated myopathy. Neuromuscul Disord. 2013; 23:418–426. [PubMed: 23489660]
10. Brooke MH, Neville HE. Reducing body myopathy. Neurology. 1972; 22:829–840. [PubMed: 4117299]
11. Tomé FM, Fardeau M. Congenital myopathy with “reducing bodies” in muscle fibres. Acta Neuropathol. 1975; 31:207–217. [PubMed: 1138529]
12. Schessl J, Zou Y, McGrath MJ, et al. Proteomic identification of FHL1 as the protein mutated in human reducing body myopathy. J Clin Invest. 2008; 118:904–912. [PubMed: 18274675]
13. Gueneau L, Bertrand AT, Jais JP, et al. Mutations of the FHL1 gene cause Emery-Dreifuss muscular dystrophy. Am J Hum Genet. 2009; 85:338–353. [PubMed: 19716112]
14. Schoser B, Goebel HH, Janisch I, et al. Consequences of mutations within the C terminus of the *FHL1* gene. Neurology. 2009; 73:543–545. [PubMed: 19687455]
15. Windpassinger C, Schoser B, Straub V, et al. An X-linked myopathy with postural muscle atrophy and generalized hypertrophy, termed XMPMA, is caused by mutations in FHL1. Am J Hum Genet. 2008; 82:88–99. [PubMed: 18179888]
16. Figarella-Branger D, Putzu GA, Bouvier-Labit C, et al. Adult onset reducing body myopathy. Neuromuscul Disord. 1999; 9:580–586. [PubMed: 10619716]
17. Schessl J, Taratuto AL, Sewry C, et al. Clinical, histological and genetic characterization of reducing body myopathy caused by mutations in FHL1. Brain. 2009; 132:452–464. [PubMed: 19181672]
18. Selcen D, Bromberg MB, Chin SS, et al. Reducing bodies and myofibrillar myopathy features in FHL1 muscular dystrophy. Neurology. 2011; 77:1951–1959. [PubMed: 22094483]
19. Liewluck T, Hayashi YK, Ohsawa M, et al. Unfolded protein response and aggresome formation in hereditary reducing-body myopathy. Muscle Nerve. 2007; 35:322–326. [PubMed: 17099882]

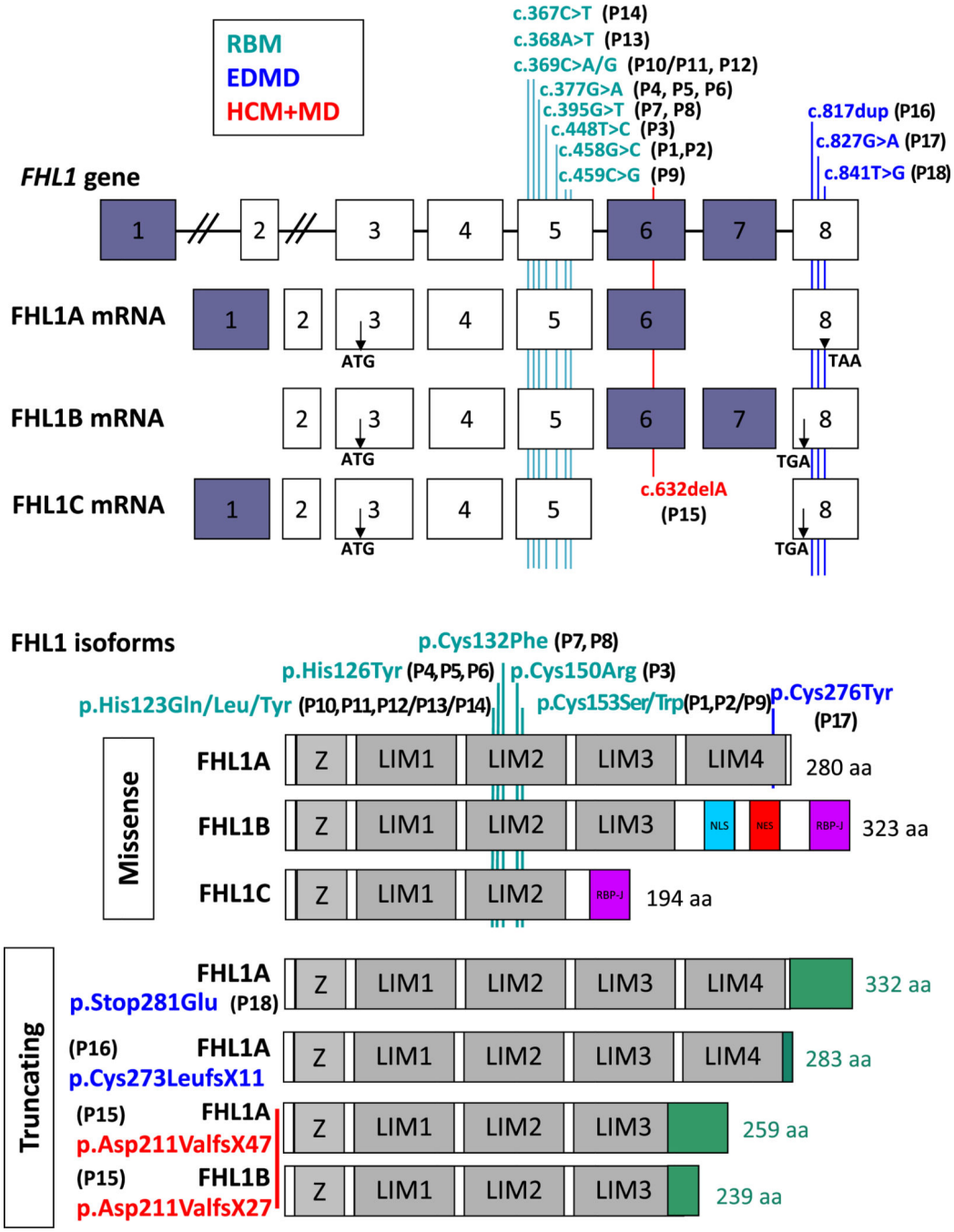

FIGURE 1.

Distribution of mutations along the *FHL1* gene, corresponding transcript isoforms, and their consequences on the 3 FHL1 protein isoforms. (Top panel) The *FHL1* gene gives rise by alternative splicing to 3 major transcribed isoforms FHL1A, B, and C. Dark gray squares represent alternatively spliced exons. Translational start (ATG) and stop (TAA or TGA) codons are indicated for the 3 FHL1 isoforms. The *FHL1* mutations identified in reducing body myopathy (RBM) patients are depicted in light blue (with corresponding family number in parentheses), in dark blue for Emery-Dreifuss muscular dystrophy (EDMD-

phenotype) patients, and in red for the hypertrophic cardiomyopathy and muscle hypertrophy (HCM + MD) patient. (Bottom panel) The 3 FHL1 protein isoforms are represented at the top of the panel, with indication of the position of the missense mutations. Below are presented the putative consequences at the protein level of the missense mutation suppressing the FHL1A stop codon and the 3 truncating mutations.

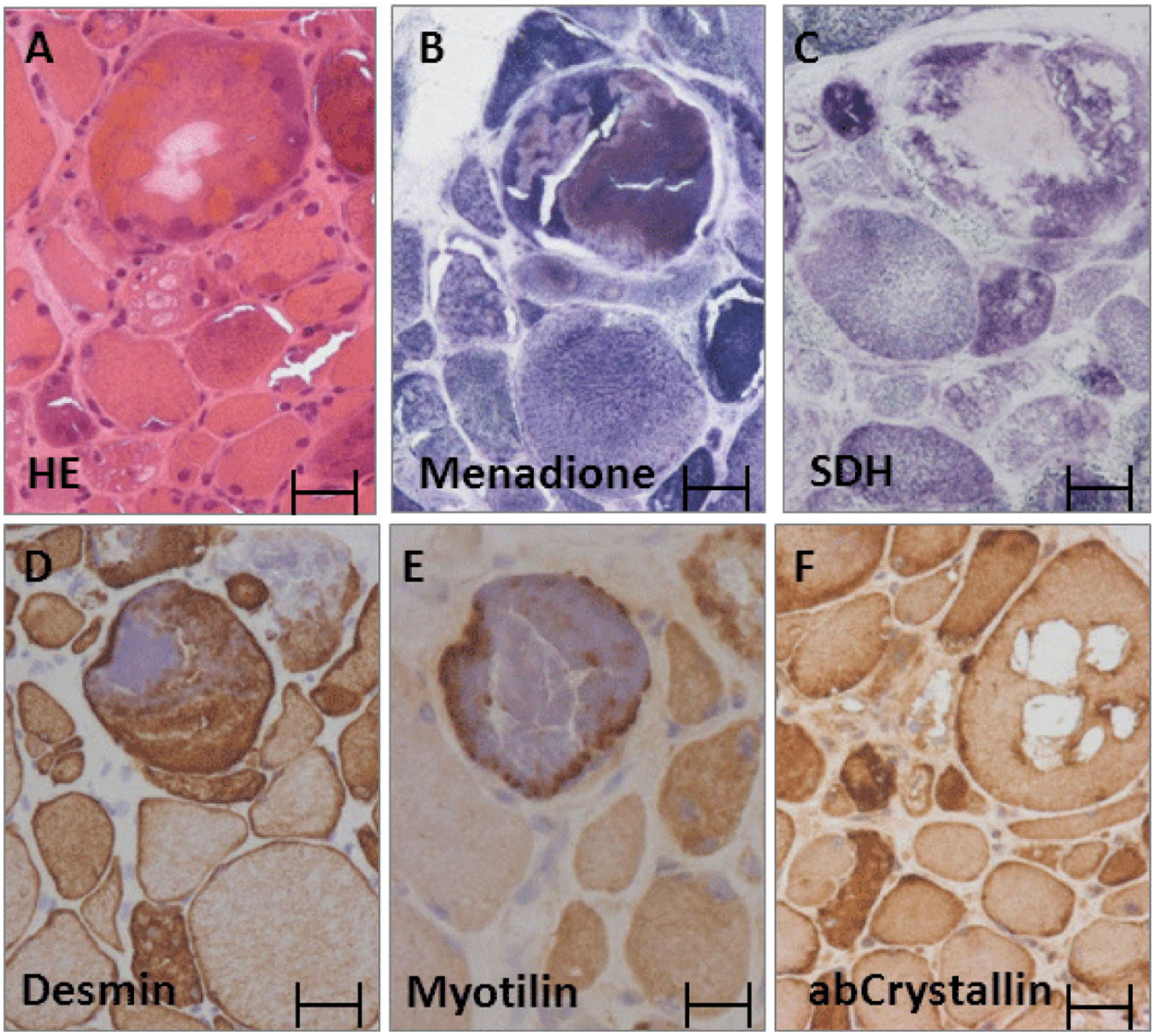

FIGURE 2.

Light microscopy and histochemistry of muscle in reducing body myopathy. Serial transverse muscle sections from patient P1 muscle biopsy. **(A)** Reducing bodies (RBs) appear as bright pink cytoplasmic inclusions on H&E. **(B)** Reducing bodies are labeled blue strongly with the reducing nitro-blue tetrazolium (NBT)–menadione reaction; **(C)** they do not stain for succinic dehydrogenase (SDH). **(D–F)** Desmin, αB-crystallin, and myotilin are not found inside RBs. Scale bar = **(A–F)** 20 μm.

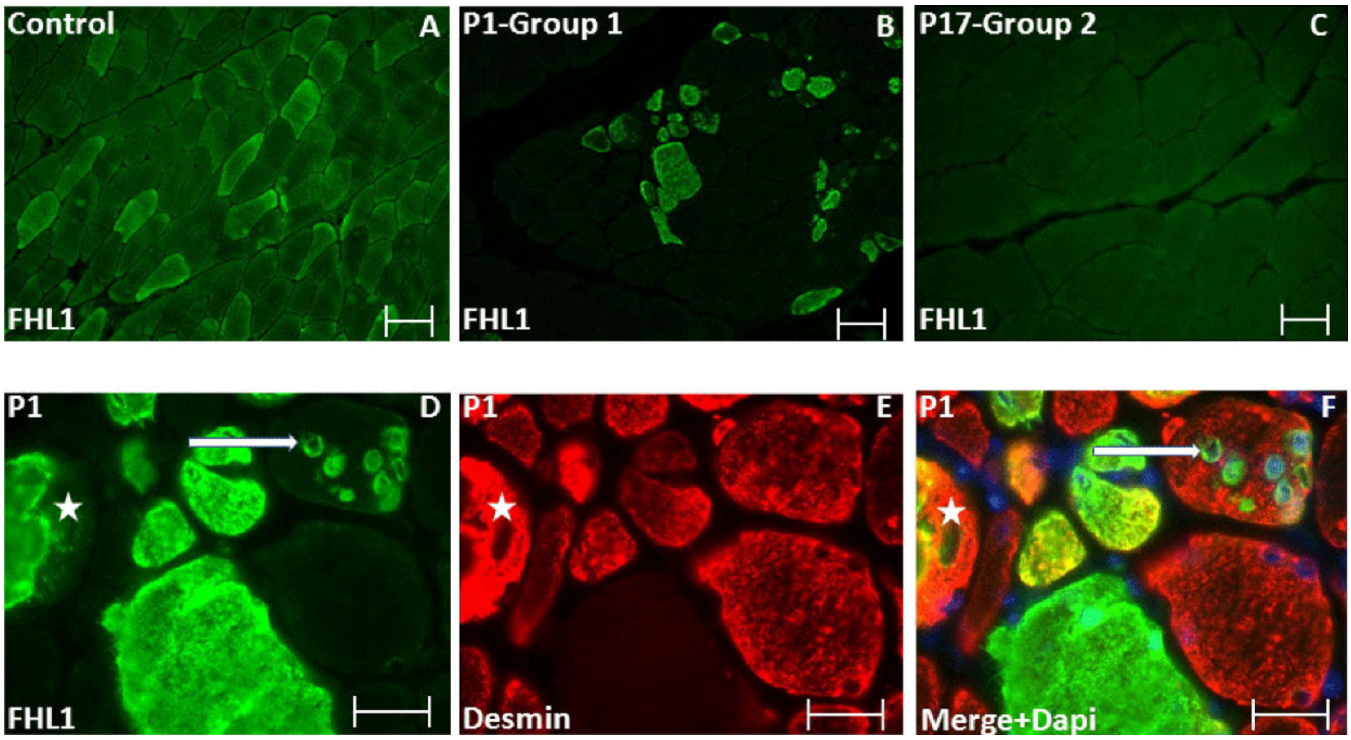

FIGURE 3.

Immunofluorescence of muscle in a control and in reducing body myopathy. **(A)** FHL1 immunofluorescence in a control muscle shows localization of the protein to the sarcomere. **(B)** In a muscle section from patient P1, FHL1 immunoreactivity is absent in normal fibers but there is intense staining of atrophic fibers or in fibers containing reducing body (RB) material. **(C)** Patient 17 from Group 2 shows a homogeneous but less intense FHL1 pattern versus the control muscle. **(D–F)** Intracytoplasmic inclusions corresponding to RBs are strongly labeled with an anti-FHL1 antibody **(D)**. Desmin immunoreactivity is found at the periphery of the RBs but not inside them (white stars in **D–F**). In particular, desmin accumulation seems to form a scaffolding structure around RBs **(D, F)**. Double labeling immunofluorescence analysis using antibodies against FHL1 and desmin **(F)**. There is increased FHL1 immunoreactivity around myonuclei (arrows in **[D]** and **[F]**). Scale bar = **(A–F)** 20 μm.

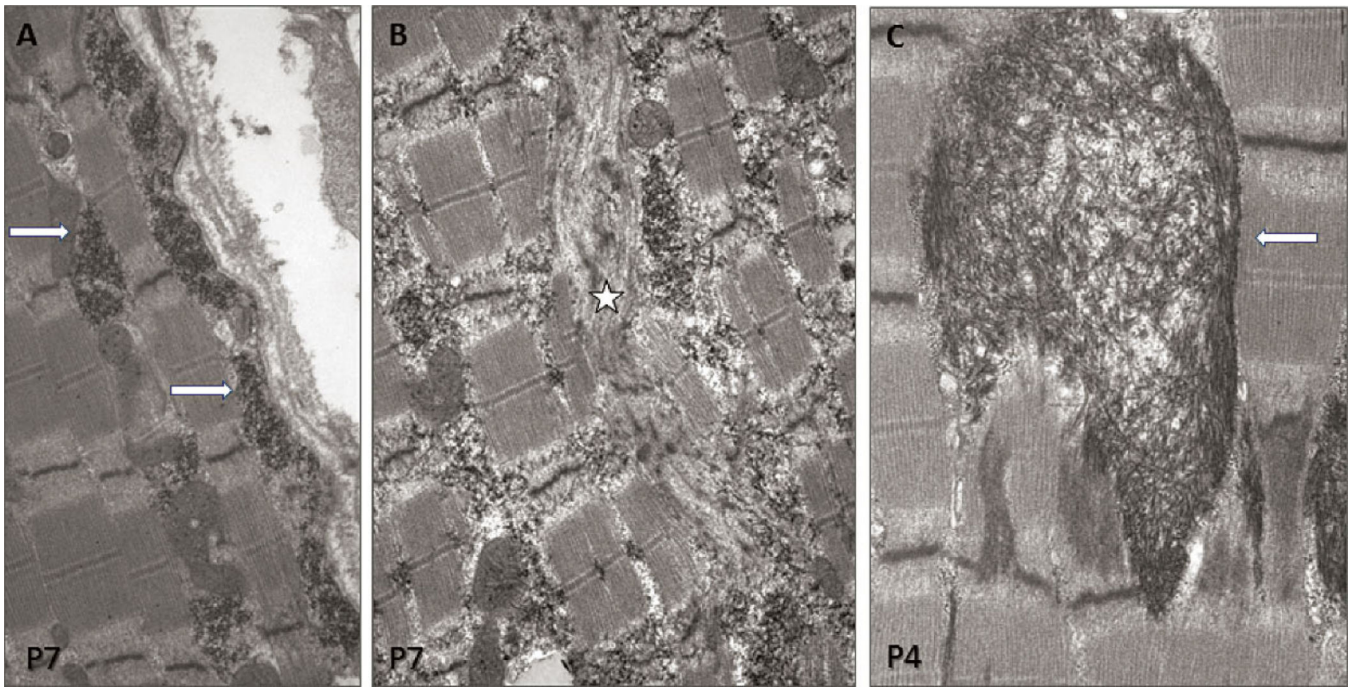

FIGURE 4.

Electron microscopy of muscle in reducing body (RB) myopathy. **(A)** Highly osmiophilic granular material seems to emanate from the I-band (indicated by arrows). **(B)** Fine filamentous semidense material is observed near the Z-line and extending along the sarcomere (indicated by a star). **(C)** RB material corresponds to coarse tubulofilaments (indicated by an arrow). Original magnification: **(A)** 14,000×; **(B)** 14,800×; **(C)** 21,500×.

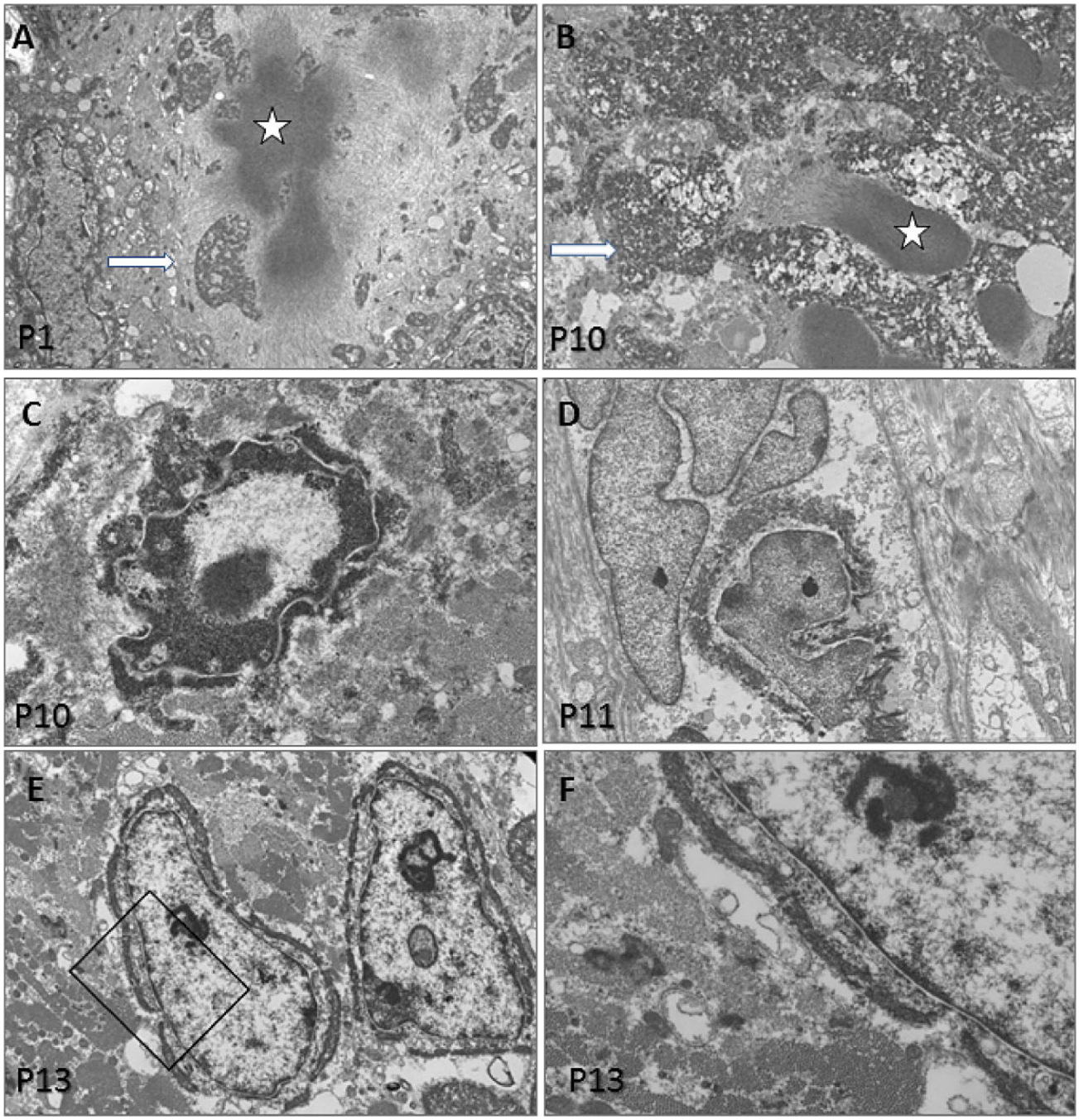

FIGURE 5.

Electron microscopy of muscle in reducing body (RB) myopathy. **(A, B)** Typical cytoplasmic bodies (stars) with a dense core and a clear halo of fine filaments surround or are intermingled with the RBs (arrows). **(C–F)** Osmiophilic tubulofilamentous material corresponding to RBs is consistently localized around myonuclei. **(F)** Higher power image of **(E)**. Original magnification: **(A)** 14,000×; **(B)** 21,500×; **(C)** 21,800×; **(D)** 21,000×; **(E)** 32,000×; **(F)** 110,000×.

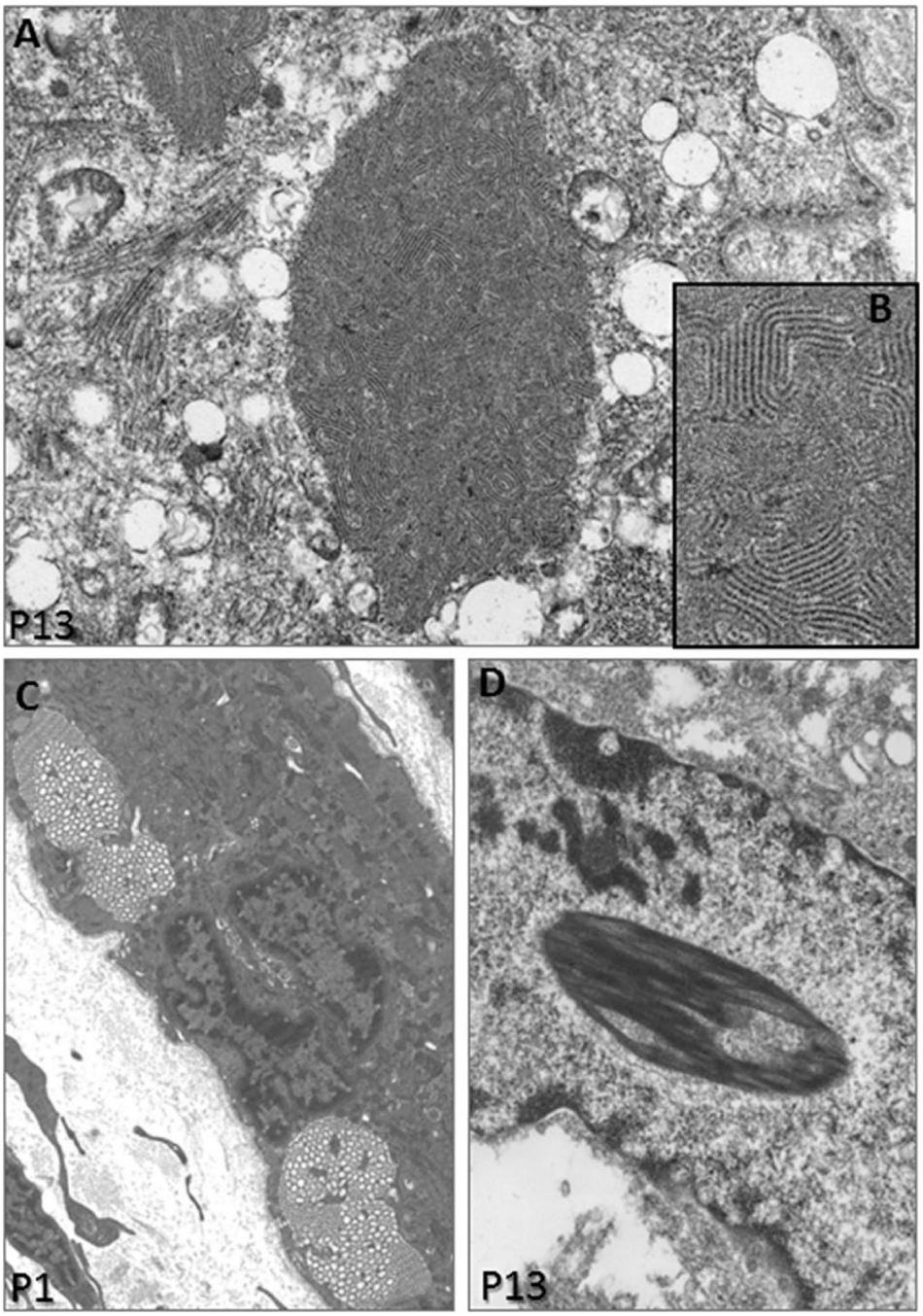

FIGURE 6.

Electron microscopy of muscle in reducing body myopathy. **(A, B)** Fingerprint bodies. **(B)** Higher magnification of **(A)**. **(C)** Dilated sarcotubular cisternae. **(D)** Intranuclear rod. Original magnification: **(A)** 14,300×; **(B)** 45,000×; **(C)** 6,000×; **(D)** 14,000×.

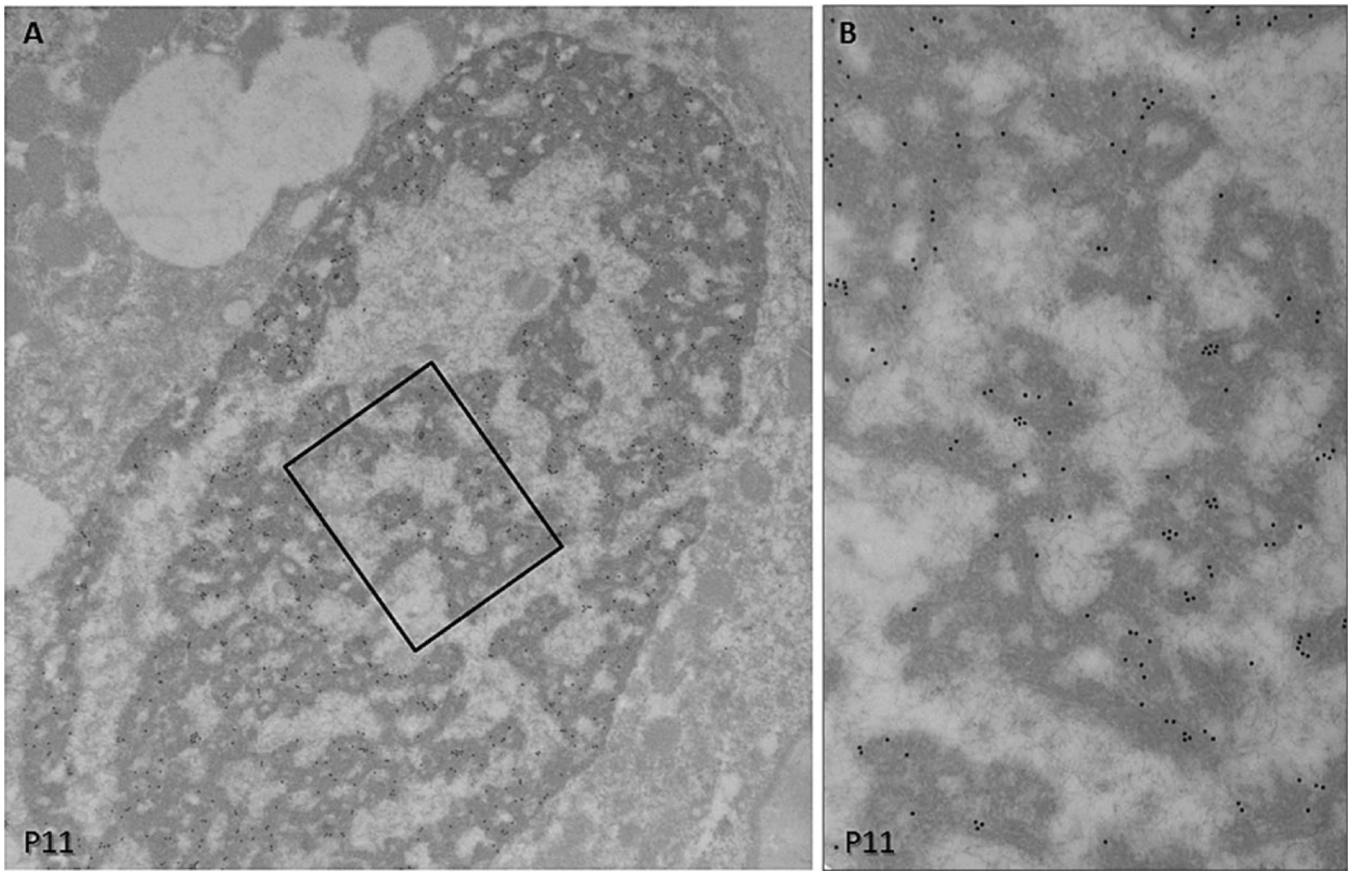

FIGURE 7.

Immunoelectron microscopy of muscle in reducing body (RB) myopathy. **(A, B)** Gold-labeled anti-FHL1 antibody label is strongly enriched in the electron-dense inclusion corresponding to an RB. **(B)** Higher magnification of **(A)**. Original magnification: **(A)** 13,700×; **(B)** 41,000×.

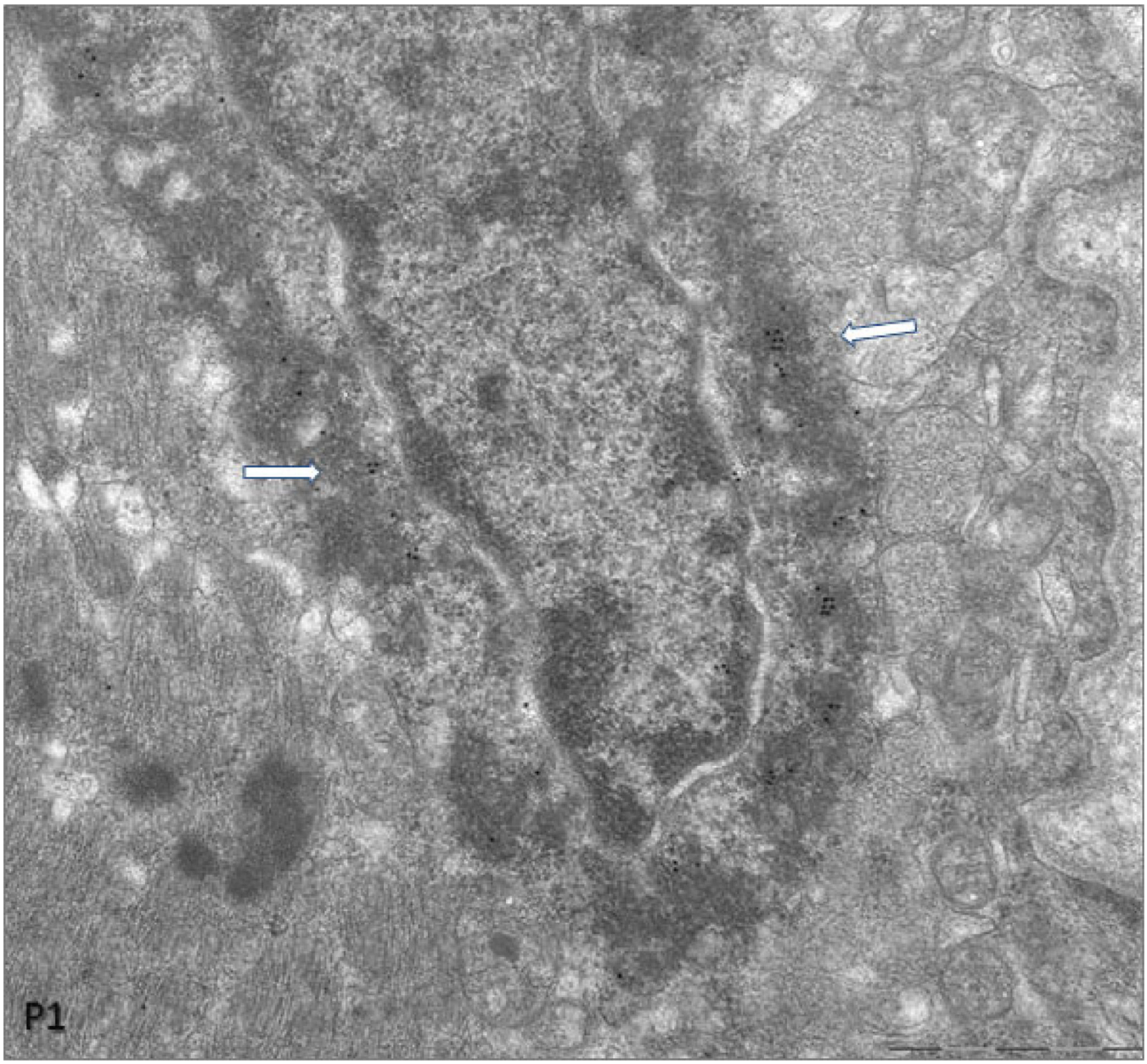

FIGURE 8.
Immunoelectron microscopy of muscle in reducing body (RB) myopathy. RB material surrounding nuclei is partly composed of FHL1. Original magnification: 18,300×.

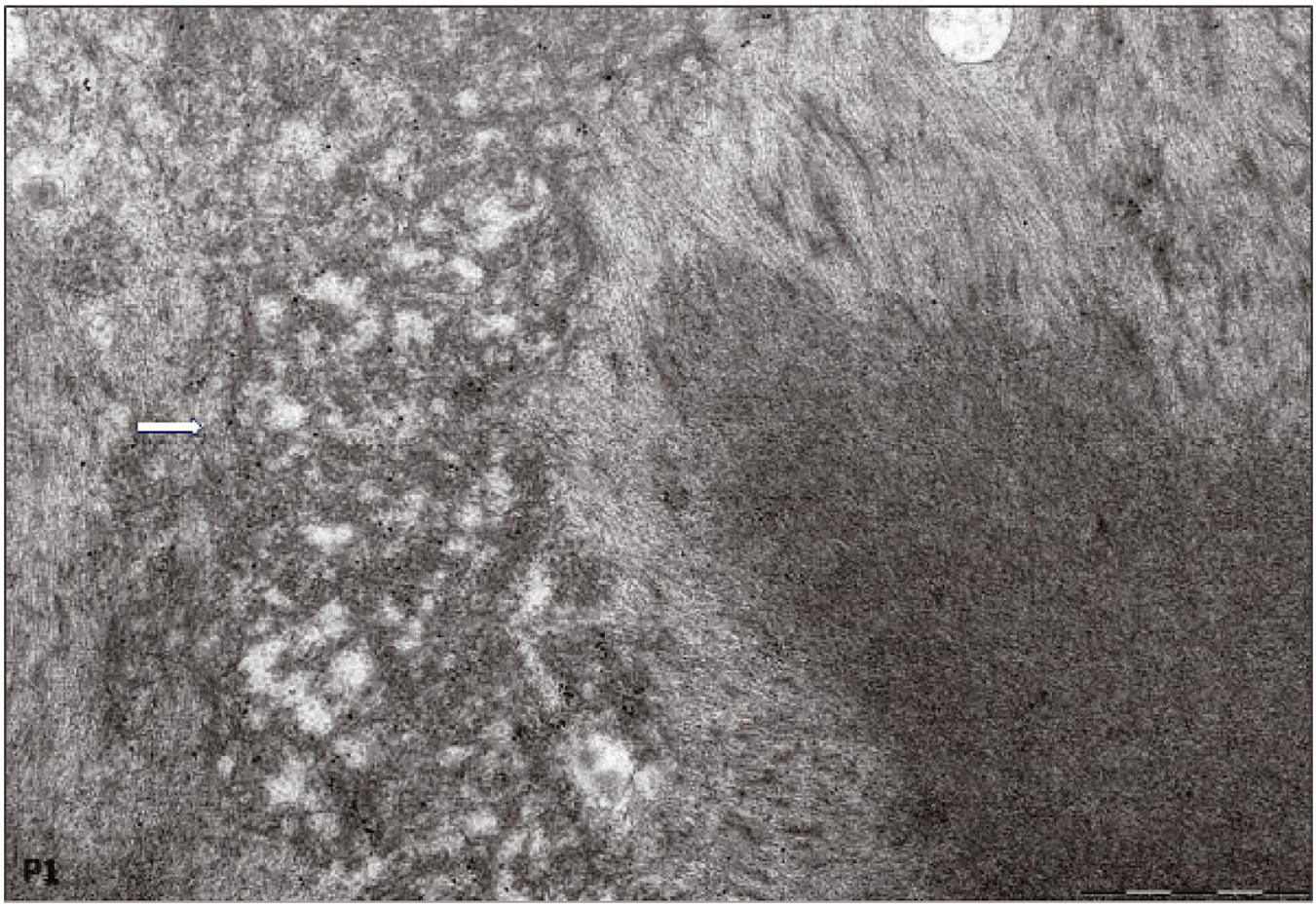

FIGURE 9.

Immunoelectron microscopy of muscle in reducing body (RB) myopathy. Cytoplasmic bodies do not show reactivity with a gold particle–labeled FHL1 antibody, whereas RB material intermingled with cytoplasmic bodies (arrow) is immunoreactive with the FHL1 antibody. Original magnification: 28,300×.

TABLE

Clinical, Laboratory, and Genetic Features of Patients

Patient Sex Current Age	Age at Onset (age at biopsy)	Biopsied Muscle	Morphologic Methods	Symptoms at Presentation/Current Symptoms/Other Relevant Findings	Affected Family Members	CK Increase Above Upper Normal	FHL1 Mutation: Nucleotide Change/Exon	FHL1 Isoform Modification	Reference
P1, F, 26 years	21 years (24 years; 25 years)	Deltoid	IHC, IF, EM, IEM	L lower limb weakness, L arm weakness/4 limb asymmetric weakness with facial involvement/ dysphagia	None	469, 3-fold	c.458G→C/ exon 5 de novo	p.Cys153Ser for the 3 isoforms FHL1A, FHL1B, and FHL1C	Present article
P2, M, 21 years	12 years (14 years)	Deltoid	IHC, EM	Rigid spine, waddling gait/proximal lower limb girdle, and distal lower limbs muscle weakness/ knees retraction	None	5,000, 29-fold	c.458G→C/ exon 5	p.Cys153Ser for the 3 isoforms FHL1A, FHL1B, and FHL1C	Present article
P3, F, 29 years	20 years (20 years)	Vastus lateralis	IHC, EM, IEM	Walking difficulties, waddling gait/lower limb girdle severe weakness	None	577, 4-fold	c.448T→C/ exon 5	p.Cys150Arg for the 3 isoforms FHL1A, FHL1B, and FHL1C	Present article
P4, F, 48 years	24 years (24 years)	Deltoid	Reappraisal of IHC, EM, IEM	L scapuloperoneal weakness/4 limb weakness	First-degree cousin	333, 2-fold	c.377G→A/ exon 5	p.Cys126Tyr for the 3 isoforms FHL1A, FHL1B, and FHL1C	(16) and present article
P5 M, 10 years	9 years	Biceps	IHC, EM, IEM	Difficulties in sport activities/axial and limb girdle weakness, distal weakness/rigid spine, mild respiratory involvement	Mother	2,000, 13-fold	c.377G→A/ exon 5	p.Cys126Tyr for the 3 isoforms FHL1A, FHL1B, and FHL1C	Present article
P6, F, 39 years	29 years (33 years; 36 years)	Vastus Lateralis	IHC, EM, IEM	Myalgias, L hand and R arm weakness/ asymmetric proximodistal weakness/rigid cervical spine	Son	450, 3-fold	c.377G→A/ exon 5	p.Cys126Tyr for the 3 isoforms FHL1A, FHL1B, and FHL1C	Present article
P7, M, 21 years	2 years (4.5 years)	Tibialis anterior	IHC, EM, IEM	Axial and limb girdle symmetric weakness/ wheelchair-bound, diffuse weakness/respiratory failure	Mother	576, 4-fold	c.395G→T/ exon 5	p.Cys132Phe for the 3 isoforms FHL1A, FHL1B, and FHL1C	Present article
P8, F, 48 years	10 years (31 years)	Deltoid	IHC, EM, IEM	Asymmetric lower limbs distal weakness upper limb girdle weakness/diffuse muscle weakness/rigid spine	Son	417, 3-fold	c.395G→T/ exon 5	p.Cys132Phe for the 3 isoforms FHL1A, FHL1B, and FHL1C	Present article
P9, F, 17 years	14 years (15 years)	Vastus lateralis	IHC, IF, EM, IEM	Asymmetric facial muscle bulk, R upper limb weakness progressed into generalized weakness/limb girdle weakness, waddling	None	686, 4-fold	c.459C→G/ exon 5	p.Cys153Trp/for the 3 isoforms FHL1A, FHL1B, and FHL1C	Present article

J Neuropathol Exp Neurol. Author manuscript; available in PMC 2017 January 04.

Patient Sex Current Age	Age at Onset (age at biopsy)	Biopsied Muscle	Morphologic Methods	Symptoms at Presentation/Current Symptoms/Other Relevant Findings	Affected Family Members	CK Increase Above Upper Normal	FHL1 Mutation: Nucleotide Change/Exon	FHL1 Isoform Modification	Reference
				gait/scoliosis					
P10, M, 7 years	1Y1.5 years (2 years)	n.d.	Reappraisal of IHC and EM, IEM	Head drop, scapular muscle amyotrophy, abolished reflexes/proximal muscle weakness, muscle hypotrophy/ resuscitated cardiac arrest at 3 years, respiratory failure	None	2,000, 13-fold	c.369C→A/ exon 5	p.His123Gln for the 3 isoforms FHL1A, FHL1B, and FHL1C	(17) (Patient 6)
P11, F, 15 years	3.8 years (5 years)	Deltoid	ME Reappraisal of IHC, IEM	Frequent falls, abnormal gait/limb girdle weakness, wheelchair-bound, dysphagia needing gastrostomy/cardiac involvement, respiratory failure	None	1,080, 7-fold	c.369C→G/ exon 5	p.His123Gln for the 3 isoforms FHL1A, FHL1B, and FHL1C	(17) (Patient 5)
P12, F, 15 years	4 years (7 years)	Deltoid	EM Reappraisal of IHC, IEM	Frequents falls/progressive proximal and axial weakness, wheelchair bounded/severe contractures, severe scoliosis	None	513, 3-fold	c.369C→G/ exon 6	p.His123Gln for the 3 isoforms FHL1A, FHL1B, and FHL1C	(17) (Patient 4)
P13, F, 10 years	4 years (6 years)	Vastus lateralis	EM Reappraisal of IHC, IEM	Frequent falls, walking difficulties, limb girdle muscular weakness/ progressive diffuse weakness/scoliosis	None	114, Normal	c.368A→T/ exon 5	p.His123Leu for the 3 isoforms FHL1A, FHL1B, and FHL1C	(17) (Patient 3)
P14, F, 9 years	4 months (10 months)	Vastus laterali	IHC, EM	Head lag/axial hypotonia/ respiratory involvement	None	349, 3-fold	c.367G→A/ exon 5 de novo	p.His123Tyr for the 3 isoforms FHL1A, FHL1B, and FHL1C	Present article
P15, M, 29 years	3 weeks (25 years)	Deltoid	IHC, IF, EM, IEM	Hypertrophic cardiomyopathy/ diffuse muscle pain/muscular hypertrophy	Maternal grandmother	600, 3-fold	c.632delA/exon 6 novel mutation	FHL1A: p.Asp211ValfsX47; FHL1B: p,Asp211ValfsX27; FHL1C: not affected	Present article
P16, M, 47 years	6 years (30 years)	Vastus lateralis	IF, EM Reappraisal of IHC.	Multiple contractures/severe axial weakness with associated mild limb girdle weakness, dysphonia, and dysphagia/rigid spine, hypertrophic cardiomyopathy, respiratory failure	None	700, 4-fold	c.817dup/exon 8	FHL1A: p.Cys273LeufsX 11; FHL1B and FHL1C not affected	(13) (F11, IV-4)
P17, M, 62 years	48 years (58 years)	Deltoid	IF, EM Reappraisal of IHC.	Lower limb girdle weakness, axial weakness, hypertrophic cardiomyopathy, cardiac arrhythmia/severe axial weakness and difficulties in walking, respiratory failure/camptocormia/ bent spine	Grandfather, 2 brothers, and 2 nephews	400, 3-fold	c.827G→A/ exon 8	FHL1A: p.Cys276Tyr; FHL1B and FHL1C not affected	(13) (F1328, II-4)

Patient Sex Current Age	Age at Onset (age at biopsy)	Biopsied Muscle	Morphologic Methods	Symptoms at Presentation/Current Symptoms/Other Relevant Findings	Affected Family Members	CK Increase Above Upper Normal	FHL1 Mutation: Nucleotide Change/Exon	FHL1 Isoform Modification	Reference
P18, M, 23 years	10 years (12 years)	Vastus lateralis	Reappraisal of IHC. IF, EM	Stiff neck/scapuloperoneal weakness, joints contractures, scoliosis/dysphonia caused by vocal palsy	Brother	Normal	c.841T→G/ exon 8	FHL1A: p.Stop281Glu; FHL1B and FHL1C not affected	(13) (F997, IV-8)

EM, electron microscopy; IEM, immunoelectron microscopy; IF, immunofluorescence; IHC, immunohistochemistry; L, left; P1 to P14, Group 1; P15 to P18, Group 2; R, right.